

Adsorbate-induced surface stress and self-assembly of $(2 \times 1)\text{O}$ on $\text{Cu}(110)$ measured with an STM

Ch. Bombis, M. Moiseeva, and H. Ibach

Institut für Schichten und Grenzflächen ISG 3, Forschungszentrum Jülich GmbH 52425 Jülich, Germany

(Received 30 March 2005; revised manuscript received 4 October 2005; published 6 December 2005)

The formation of the (2×1) oxygen stripe phase on $\text{Cu}(110)$ at room temperature is imaged *in situ* with an STM and simultaneously a quantitative determination of the oxygen-induced surface stress is accomplished. The bending bar technique is utilized with the bending measured by the STM. We find that the difference $\Delta\tau$ of the surface stresses of the $(2 \times 1)\text{O}$ phase on $\text{Cu}(110)$ and the clean $\text{Cu}(110)$ surface is compressive for both directions, which is in accordance with the adsorption of oxygen on other surfaces. The stress depends significantly on the coverage. Quantitative aspects of these results raise an interesting issue concerning the applicability of the Marchenko-Alerhand continuum model for the self-assembly of the stripe phase.

DOI: 10.1103/PhysRevB.72.245408

PACS number(s): 68.35.Gy, 68.37.Ef, 68.43.Hn, 68.47.De

I. INTRODUCTION

Stress in thin-film systems and surface stress plays a decisive role in self-assembled pattern formation (for a review see, e.g., Refs. 1–5 and references therein). The very first observation of self-assembly into an ordered pattern by Kern *et al.*⁶ in 1991 was for the $(2 \times 1)\text{O}$ phase on $\text{Cu}(110)$ which orders into a stripe pattern. Later this ordering was explained by the principle of stress domain self-assembly⁷ discovered earlier by Marchenko⁸ and Alerhand *et al.*⁹ Recently, Prévot *et al.*^{10,11} analyzed the strain field on the striped phase using grazing incidence x-ray scattering. By a comparison of theoretical modeling with x-ray intensities Prévot *et al.* showed that the strain field can be understood as originating from a different surface stress of the oxygen covered and the clean surface. In their work they find this difference $f_{[1\bar{1}0]} = \tau_{\text{O}[1\bar{1}0]} - \tau_{\text{Cu}[1\bar{1}0]} = (-1.0 \pm 0.1) \text{ N m}^{-1}$ to be independent of the coverage in the range between 0.51 and 0.76. However, until now no direct measurement of the oxygen induced surface stress exists. We have therefore performed measurements of the induced surface stress using the bending bar technique and the scanning tunneling microscope (STM) for the detection of the bending and the simultaneous investigation of the structure and the determination of the surface coverage. The induced stress orthogonal to the stripes and parallel to the stripes was measured in the whole coverage interval, i.e., from $0 \leq \theta_S \leq 1$. In contrast to Prévot *et al.*, we find a significant dependence of the stress on the coverage. The result for the stress difference orthogonal to the stripes is used for a quantitative analysis of the stripe periodicity.

The paper is organized as follows. The theoretical aspects of the bending bar technique, the relevant equations, and data for our experimental set up are collocated in the following section. The experimental part is divided into two sections. In the first part, the preparation of the samples and the formation of the system $(2 \times 1)\text{O}$ on $\text{Cu}(110)$ is presented. The second part describes the bending bar experiment applied to our experimental setup in more detail. Furthermore, a comprehensive and critical description of the analysis of STM images regarding the bending information is presented. With

the results of these bending measurements, an analysis regarding the stress is performed in Sec. V. Experimental results concerning the stripe periodicity and their analysis are presented in Sec. VI. In Sec. VII, we compare our result to previous investigations and discuss effects of the kinetics on the ordering process. Conclusions and a short summary are presented in Sec. VIII.

II. THEORETICAL ASPECTS OF THE BENDING BAR TECHNIQUE FOR ANISOTROPIC SURFACES

The functional principle of the bending bar technique is based on the bending of a thin bar due to a change in the surface stress on one of the two sides of the bar. Figure 1 illustrates schematically how the bending is induced by an adsorption process on one side of the bar as well as the measurement of the bending by the STM.

For a quantitative determination of the induced surface stress, one needs a relationship between the stress and the bending of the bar. For an isotropic material and an isotropic surface stress the relationship between bending and surface stress is described by the so-called Stoney equation.¹²

$$\Delta\tau = \frac{Yt^2}{6R(1-\nu)}. \quad (1)$$

Here Y denotes Young's modulus, t the thickness of the bar, ν the Poisson number, and R the radius of curvature. The

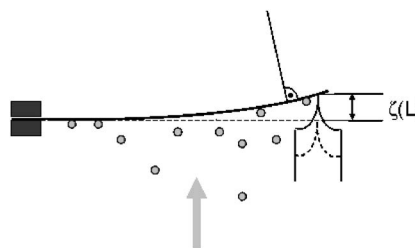


FIG. 1. Due to an adsorption process on the bottom side of the bar, the surface stress on this side changes, and the crystal bends (upwards in this example). The bending $\zeta(L)$ is measured by the STM tip, which follows the bending sample at the end of the bar if operating in the constant-current mode. The bar is fixed on the left side.

Stoney equation was generalized to the case of surfaces on crystals with at least C_{2v} symmetry² using the principle of energy minimization (see also Ref. 13):

$$\begin{aligned}\Delta\tau_1 &= \frac{t^2}{6(s'_{11}s'_{22} - s'^2_{12})}(s'_{22}\kappa_1 - s'_{12}\kappa_2), \\ \Delta\tau_2 &= \frac{t^2}{6(s'_{11}s'_{22} - s'^2_{12})}(s'_{11}\kappa_2 - s'_{12}\kappa_1).\end{aligned}\quad (2)$$

Here, the two orthogonal directions of the plate are denoted with the indices 1 and 2, respectively, and s'_{ij} are elastic constants in an appropriate coordinate system, which is adapted to the experimental side conditions. These crystallographic directions have to be specified according to the surface under investigation. For some surface orientations, the result of this tensor transformation is listed in Ref. 4, for a general treatment of this problem see Ref. 14. Here we are interested in the (110) surface. Denoting the two orthogonal directions on this surface, $[1\bar{1}0]$ and $[001]$ as 1 and 2, respectively, one obtains

$$\begin{aligned}s'_{11} &= \frac{1}{2}s_{11} + \frac{1}{2}s_{12} + \frac{1}{4}s_{44}, \\ s'_{12} &= s_{12}, \\ s'_{22} &= s_{11}.\end{aligned}\quad (3)$$

With the elastic constants of copper at room temperature, i.e., 20 °C, we find¹⁵ $s_{11}=15.0\times 10^{-12}$ m²/N, $s_{12}=-6.3\times 10^{-12}$ m²/N, and $s_{44}=13.3\times 10^{-12}$ m²/N, respectively. Finally with Eq. (3) we calculate $s'_{11}=7.68\times 10^{-12}$ m²/N, $s'_{12}=-6.3\times 10^{-12}$ m²/N, and $s'_{22}=15.0\times 10^{-12}$ m²/N. An important consequence of the system of two linear equations (2) is that each stress component is determined by the bending of bars along both directions and vice versa. This implies that for a quantitative analysis of the induced surface stress on an anisotropic surface one has to perform two experiments, in our case one with the $[1\bar{1}0]$ and a second one with the $[001]$ direction along the bar as discussed in more detail in Sec. IV.

Equation (2) applies only the case of free bending. In an experiment, the bar has to be fixed at one end (Fig. 1). The effect of clamping on the bending can only be neglected for bars with a very large aspect ratio (length/width).^{16,17} Since

TABLE I. Correction factors for a fcc (110) Cu surface for different aspect ratios (Ref. 18). In each case the direction of the crystallographic axes lying parallel to the long side of the bar, $[1\bar{1}0]$ and $[001]$, respectively, is denoted.

Aspect ratio	X_{11}	X_{12}	X_{21}	X_{22}
	$[1\bar{1}0]$	$[1\bar{1}0]$	$[001]$	$[001]$
1.0	0.791	0.401	0.492	0.823
2.0	0.853	0.580	0.660	0.881
4.0	0.907	0.735	0.798	0.929

such single crystal bars could not be prepared from copper, the influence of the clamping on the bending of a bar need to be taken into account. Using a finite element analysis Dahmen calculated correction factors X_{ij} for several crystal materials and various aspect ratios.¹⁸ With these factors the experimentally measured principal curvatures can be expressed as

$$\begin{aligned}\kappa_1 &= \frac{6}{t^2}(s'_{11}X_{11}\Delta\tau_1 + s'_{12}X_{12}\Delta\tau_2), \\ \kappa_2 &= \frac{6}{t^2}(s'_{12}X_{21}\Delta\tau_1 + s'_{22}X_{22}\Delta\tau_2).\end{aligned}\quad (4)$$

The curvatures κ in this equation are now defined with reference to the experimental method by which the curvature is determined.¹⁶ In this work, we measure the displacement ζ and the curvature in Eq. (4) is defined as

$$\kappa = \frac{2\zeta(L)}{L^2},\quad (5)$$

in which L is the distance to the clamping. For $X_{ij}=1$, Eq. (4) describes a free two-dimensional bending of a thin plate. For $X_{11}=X_{22}=1$ and $X_{12}=X_{21}=0$ a one-dimensional bending is described. The correction factors for Cu are numerically determined for the aspect ratios (length to width) 1, 2, and 4 (Ref. 18) (Table I). Intermediate values can be obtained by interpolation.

By inversion of Eq. (4) one obtains the following system of two linear equations for the components of the stress tensor in terms of the experimentally determined displacements ζ_1 and ζ_2 :

$$\begin{aligned}\Delta\tau_1 &= \frac{\zeta_1 t_1^2}{L_1^2} \frac{s'_{22}X_{22}}{3(s'_{22}X_{22}s'_{11}X_{11} - s'_{12}X_{12}s'_{12}X_{21})} \\ &\quad - \frac{\zeta_2 t_2^2}{L_2^2} \frac{s'_{12}X_{12}}{3(s'_{22}X_{22}s'_{11}X_{11} - s'_{12}X_{12}s'_{12}X_{21})}, \\ \Delta\tau_2 &= -\frac{\zeta_1 t_1^2}{L_1^2} \frac{s'_{12}X_{21}}{3(s'_{22}X_{22}s'_{11}X_{11} - s'_{12}X_{12}s'_{12}X_{21})} \\ &\quad - \frac{\zeta_2 t_2^2}{L_2^2} \frac{s'_{11}X_{11}}{3(s'_{22}X_{22}s'_{11}X_{11} - s'_{12}X_{12}s'_{12}X_{21})}.\end{aligned}\quad (6)$$

The thickness t and the positions L where the ζ are measured are now labeled with an index, to account for different samples with slightly different geometric dimensions. The quantity $\zeta_{1,2}(t_{1,2}^2/3L_1^2)$ is denoted as the reduced bending in the following. It accounts for the geometric dimensions of the samples and permits a comparison of data obtained on different samples.

III. EXPERIMENTAL, PART I: THE (2×1)O PHASE ON CU(110)-SAMPLE PREPARATION

The single crystals used in our experiments were cut by spark erosion and polished mechanically to an accuracy of 0.1°. For cleaning the samples in vacuum, we performed

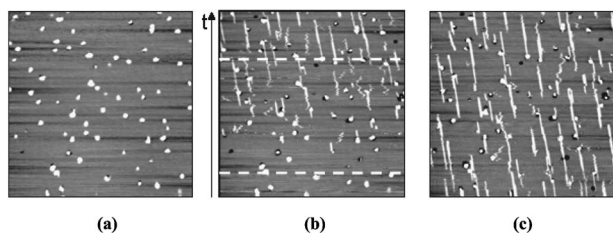


FIG. 2. Section of a terrace ($100 \times 100 \text{ nm}^2$) before (a) during (b) and after (c) exposure of the Cu(110) sample with a dose of 1.5 L oxygen (pressure $p_{\text{inlet}} \approx 1 \times 10^{-8}$ mbar, exposure time $t_{\text{inlet}} = 202$ s) at room temperature. Exposure is taking place within the time interval that corresponds to the scanned region indicated by the dashed lines in image (b). A time axis next to image (b) indicates the direction of the scanning process. ($I_T = 0.05$ nA, $U_T = 3$ V, scanning speed = 300 nm/s).

repeated cycles of sputtering with Ar^+ and successive annealing. The first sputtering process after a transfer of the sample into the chamber lasted for approximately 2 to 3 h at an ion energy of 0.5 keV and an ion current density of $5 \mu\text{A}/\text{cm}^2$. Afterwards repeated cycles of sputtering for 5 min under the same conditions as mentioned above and heating the sample for 30 min at approximately 525°C were performed. The rate of heating up or cooling down did not exceed 30°C per minute to avoid too large thermal stresses, which worsen the crystallographic quality of the surface.¹⁹ The temperature was calibrated vs the readings of a thermocouple attached to a spent copper sample in separate experiments. After a minimum of 10 cycles, no contamination was detectable in the Auger spectrum. In the last few cycles, the sputtering time was prolonged to 20 min and the heating time shortened to 20 min. As one can see in the STM images of Figs. 2(a) and 3(a), the surfaces are not perfectly clean. We suppose different sources of this imperfection, but mainly we believe, that the annealing temperature is too low for a complete leaching of the crystal. We have restricted ourselves to 700°C by repeating cycles and 525°C by the last cycle, since we have found that the samples are crystallographically destroyed by annealing it at a higher temperature. We suppose that this is

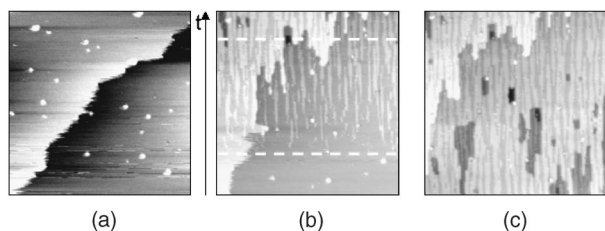


FIG. 3. Section of the Cu(110) sample ($100 \times 100 \text{ nm}^2$) before (a) during (b) and after (c) exposure of the sample with a dose of 10 L oxygen $p_{\text{inlet}} \approx 1 \times 10^{-8}$ mbar, $t_{\text{inlet}} = 22$ min 15 s) at room temperature. Exposing is taking place within the time interval corresponding with the scanning interval indicated by the dashed lines in image (b). A time axis next to image (b) indicates also the direction of scanning. Due to the growth mechanism of the added rows, the step edge is eaten up and even holes are generated on the terrace, as visible in image (c). ($I_T = 0.05$ nA, $U_T = 3$ V, scanning speed = 50 nm/s).

either due to the large thermal gradient between the sample mount and the rest of the sample or caused by the growth of dislocations from the clamping position.

To prepare the samples for a bending bar experiment one has to take care, that adsorption of oxygen takes place on one side of the bar only. In our set up of the sample holder, we are not able to control the backside of the sample with any analytical technique such as AES or STM. However, we assume the backside of the sample to remain contaminated with C and S. The backside should therefore be relatively inert. To further ensure that oxygen adsorbs only on one side of the sample during the bending bar experiment, we exposed the sample with 20 L oxygen at $p_{\text{inlet}} \approx 1 \times 10^{-7}$ mbar for $t_{\text{inlet}} = 267$ s prior to each experiment. This dose is beyond the value for obtaining a full coverage. The exposure is followed by one cycle of sputtering and annealing on the front of the sample.

Figures 2 and 3 display a series of three consecutive STM images before, during and after exposure of the sample to oxygen, respectively. In addition to some remaining impurities, visualized as bright spots, one starts from an approximately clean surface. The surface was exposed to oxygen in the time span between the scan lines indicated by dashed white lines in Figs. 2 and 3. In this period, single CuO strings nucleate and are imaged as sidled lines due to place exchange processes on the terrace. Later on these single strings agglomerate to form a stripe shaped domain of $(2 \times 1)\text{O}$ (Ref. 20) on Cu(110). These stripes are distributed rather homogeneously over the surface. In particular, the second series affirms due to the retraction of the step edge position in Fig. 3(b) once again²¹⁻²³ rather nicely that Cu adatoms are removed from the step edges to build an added row structure. In a deficiency of adatoms from the step edges, in some cases the adatoms are even generated by an extraction from the flat terrace, which generates holes there, as visible in Fig. 3(c).

IV. EXPERIMENTAL, PART II: THE BENDING BAR EXPERIMENT

As explained in detail in the theoretical chapter, two different experiments with the bending bar technique need to be performed. Figure 4 illustrates our experimental set up schematically: In this view, the observer looks onto the samples from the bottom. The STM tip is sketched as a circle with a point denoting the end of the tip. The samples are clamped on the left side. The crystallographic orientations are labeled and the relative orientation of the oxygen stripe phase is indicated by grey stripes. The geometric dimensions of the crystals are measured with a light microscope with an accuracy of 0.01 mm and listed in Table II, respectively.

Due to difficulties concerning the tip approaching procedure and crystallographic imperfections at the very end of the bar, the measurement point deviates slightly from the edge, as shown also in Fig. 4. For a calculation of the aspect ratio and the determination of the magnitude L of Eq. (6) we therefore used L_{exp} , which is the real distance of the measurement point to the clamping instead of the total length of the bar.

The experiments were performed as follows: After the cleaning and preexposure procedures, scanning with the

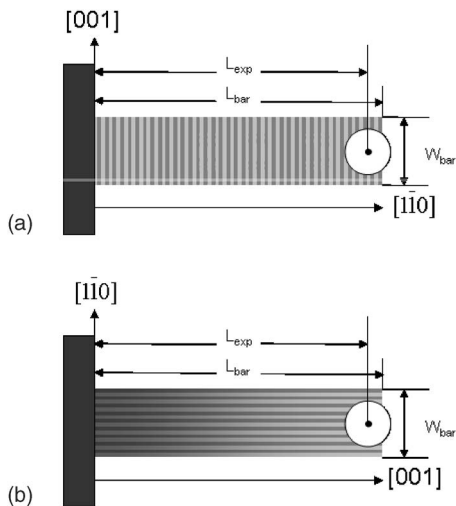


FIG. 4. Schematic drawing of the bending bar experiments visualized from the bottom side of the sample. The clamping is indicated on the left side as a grey rectangle, the STM tip as a circle shaped pole and a point shaped end of the tip. The directions 1 and 2 in Eq. (6) correspond to the crystallographic directions $[1\bar{1}0]$ and $[001]$. The relative orientation of the oxygen stripe phase is also indicated by grey stripes orthogonal (a) or parallel (b) to the long side of the bar.

STM began. Scanning was continued until the residual drift, especially in the z direction, had nearly vanished or was at least very small and constant in time. Thermal stability is a necessary requirement in particular for these experiments to distinguish a bending signal from thermal drift. The scan speed and other scan parameters were matched to the intended exposure time such that an exposure was completed within one third to one half of the time required to scan the complete image. We utilized two procedures for exposing: In one procedure (method I) we continually exposed the clean sample to an appropriate oxygen dose, i.e., approximately 10 L, to obtain a full coverage within the registration time of one image. In a second procedure (method II), consecutive exposures were performed in such a way, that a nearly drift free imaging served as a starting condition for a next exposure until a full coverage was obtained after several exposures. Only one exposure was performed within the registration time of one image in either case. Both methods lead to the same results, i.e., to nearly the same bending at equal coverage. The doses were quantified by registration of the

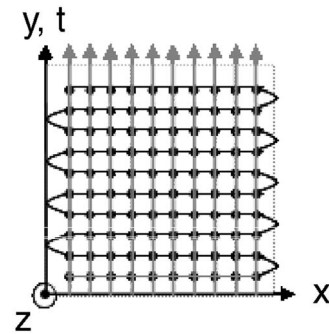


FIG. 5. Data structure of an STM image with 10×10 data points. Due to the meandering scanning path across the x - y plane, line profiles in the y direction, indicated by grey arrows, correspond in a good approximation to one common time axis.

gas inlet pressure and time, or by recording the ion current at mass 32 of a mass spectrometer. The calibration of this ion current was performed with an ionization manometer. The coverage of the stripes was determined with the help of STM images recorded after exposing.

To extract the bending of the crystal from the STM images we analyzed line profiles in the direction corresponding to the time axis, averaged over the entire image. Figure 5 illustrates an example of the data structure of an STM image with 10×10 data points. The scanning path is meandering across the x - y plane. The time difference between data points within one row is small compared to the time difference between data points of different rows. This means that to a good approximation, all data points of one row belong to one common time point, and therefore all line profiles in the y direction correspond to one common time axis. In the sketched example, averaging is performed over ten grey-colored line profiles. In the case of our STM images, composed of 512×512 pixels, averaging was performed over 512 lines. From a careful visual observation of the assigned scan line number, which is recorded at a certain time, we know approximately at which scan line the gas inlet has begun. This line correlates with the change in the slope of line profiles analyzed.

Figure 6 presents an example of an averaged line profile of an image when a gas inlet was performed during the recording time. The image size was $100 \times 100 \text{ nm}^2$ as in all further experiments presented here. The dose was 10 L and the long side of the bar ($C_{[001]I}$) was parallel to the $[001]$ direction. Starting with a small linear negative slope due to

TABLE II. Geometrical dimensions of the used crystals are listed. The index of a crystal C denotes the orientation of its long side.

Crystal	L_{bar} Length of the bar	L_{exp} Distance: measurement point- clamping	W_{bar} Width of the bar	$a=L_{\text{exp}}/W_{\text{bar}}$ (Aspect- ratio)	t Thickness of the bar
$C_{[1\bar{1}0]}$	4.33 mm	3.93 mm	1.15 mm	3.42	0.15 mm
$C_{[001]I}$	4.45 mm	4.1 mm	1.20 mm	3.42	0.082 mm
$C_{[001]II}$	4.76 mm	4.35 mm	1.61 mm	2.7	0.25 mm

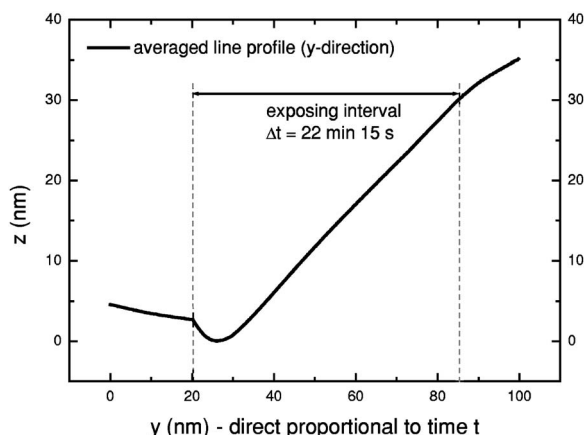


FIG. 6. Averaged line profile of an STM image registered during an exposure of a Cu(110) bending bar sample ($C_{[001]I}$) with the long side of the bar parallel to the $[001]$ direction to a dose of 10 L oxygen. Note that the y axis corresponds to the time axis. Obviously the slope of the line profile changes significantly, when the gas inlet starts and very little noticeable when it stops. The measured variation in z of several ten nm is much larger than the height of any topographic feature. Surprisingly the slope changes its sign during the gas inlet, which cannot be attributed to a bending behavior. This makes the interpretation of the bending curves nontrivial as discussed in the text.

some inclination of the sample or some residual linear drift, the slope changed sharply when the gas inlet started, as indicated by the first dashed line. At first, the slope is negative but changes continuously to positive values with increasing time. At the end of the exposure time, the slope changes again. We note that the observed changes in z are much larger than z variations in due to the topology of the sample (Figs. 2 and 3).

At first we tended to interpret the observed z deviation as the bending ζ wondering about the strange behavior of even changing the direction of bending. In the course of the experiments, we learned that there is a second source that produces a faked change in ζ which is a length change of the piezoceramics upon exposure to oxygen. In general, we could observe an elongating effect of oxygen to the piezos. While scanning in the constant-current mode, the elongation is avoided by applying an appropriate voltage on the piezo, which leads to a faked bending in the positive z direction. The experimental difficulty imposed by this artifact is that it depends on the inlet pressure and time, and the change in length continues to creep after the exposure has been terminated. Furthermore, it even changes its behavior in long ranges of time, i.e., within several months. On the other hand, in repetitive exposures of a crystal, which is completely covered, we found the faked bending to be quite reproducible. If the relevant experiments are performed within a smaller time span of several days or weeks, the behavior of the artifact did not change. An averaged faked bending could therefore be determined and subtracted from the raw data to obtain the real bending of the sample. Additionally we found in several experiments that at an inlet pressure of approximately 1×10^{-7} mbar, the faked bending nearly vanished. Comparing a corrected bending graph with uncorrected

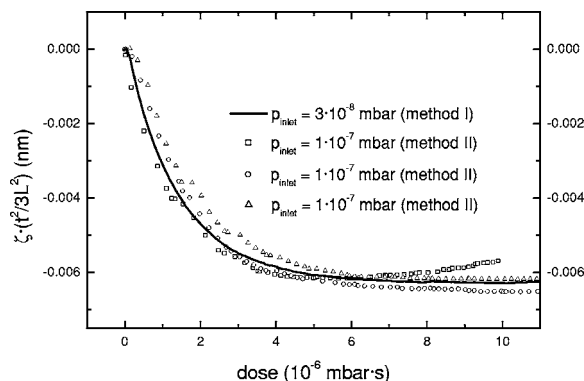


FIG. 7. Reduced bending graphs for different experiments at samples with the long side of the bar parallel to the $[001]$ direction. In several experiments with crystal $C_{[001]I}$ the gas inlet is performed with method I at an gas inlet pressure $p_{inlet} \approx 3 \times 10^{-8}$ mbar. The averaged bending curve was corrected by the faked bending as explained in the text. The resulting curve is plotted as a solid line. In experiments with crystal $C_{[001]II}$ the gas inlet is performed with method II at an gas inlet pressure $p_{inlet} \approx 1 \times 10^{-7}$ mbar. At this inlet pressure, the faked bending nearly vanishes, and therefore the plotted bending graphs pieced together from several measurements did not undergo any further correction.

bending graphs recorded at this inlet pressure, we obtained a nice accordance of the data, as can be seen in Fig. 7. In several experiments adsorption of oxygen took place on crystal $C_{[001]I}$ at $p_{inlet} \approx 3 \times 10^{-8}$ mbar. The exposure was performed with method I, i.e., a dose of 10 L is let into the chamber within the registration time of one STM image. An averaged bending graph is corrected by the faked bending, determined in separate experiments on a completely with $(2 \times 1)O$ covered sample, and plotted against the coverage. In three different experiments with the crystal $C_{[001]II}$ adsorption of oxygen took place at $p_{inlet} \approx 1 \times 10^{-7}$ mbar. The exposure was performed with method II. The plotted bending graphs are therefore pieced together from several measurements. As mentioned before, the faked bending vanished at these conditions. Therefore, we immediately obtain the real bending from a measurement and hence, no further correction of the data is necessary in this case.

To present the results as a plot of the reduced bending against the coverage, we performed a calibration of the oxygen doses vs the coverage. For this, the coverage after an exposure to oxygen is determined by analyzing STM images.

V. EXPERIMENTAL RESULTS AND DATA ANALYSIS, PART I: THE BENDING AND THE CALCULATION OF THE STRESSES

The experimental result in terms of the bending measurements is plotted in Fig. 8 as the reduced bending for the two directions against the coverage, respectively. In the course of experiments to determine the faked bending we exposed an initially oxygen free sample ($C_{[1\bar{1}0]}$) with the long side of the bar parallel to the $[1\bar{1}0]$ direction piecewise to oxygen until the surface was completely covered. Exposure was continued then for several times. From a comparison of the averaged

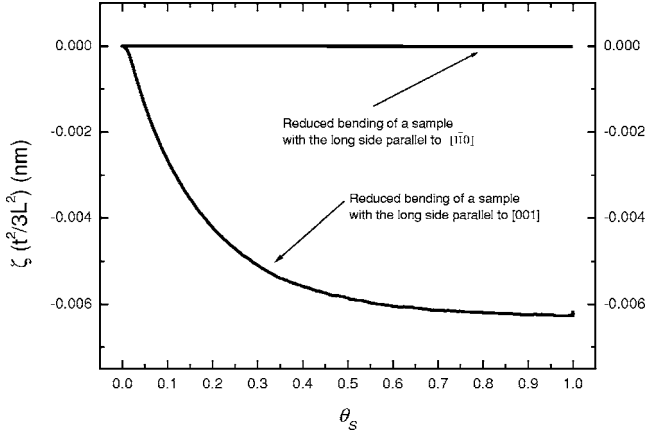


FIG. 8. Reduced bending at samples with the long side of the bar parallel to the [001] direction as well as parallel to the $[1\bar{1}0]$ direction. The nearly vanishing bending of samples with the long side of the bar parallel to the $[1\bar{1}0]$ direction does not imply that the stress is also zero.

line profiles extracted from STM images of the sample at lower coverage and the completely covered surface we learned, that the real bending of this sample nearly vanished. Therefore, we set the reduced bending of a sample with the long side of the bar parallel to the $[1\bar{1}0]$ direction, i.e., orthogonal to the oxygen stripes, to be nearly zero here. As we will see later, the vanishing bending does not imply a vanishing stress along this direction. The drawn through graph of the reduced bending from Fig. 7 is used as an averaged reduced bending of a sample with the long side of the bar parallel to the [001] direction, i.e., parallel to the oxygen stripes, and therefore plotted again in Fig. 8 vs the coverage. The reduced bending is negative. The slope of the graph is relative large in the coverage interval from $\theta_s=0$ to 0.3. For a larger coverage, the reduced bending saturates.

With two solutions of a reduced bending, the system (6) of two linear equations was solved for the corresponding stresses. The correction factors for the experimental aspect ratios a_1 and a_2 were calculated from the listed values (Table I) by fitting to an exponential function that has the correct asymptotic limit for large aspect ratios:

$$\begin{aligned} X_{11} &= 0.932 - 0.252 \exp(-a_1/1.718), \\ X_{12} &= 0.805 - 0.725 \exp(-a_1/1.706), \\ X_{21} &= 0.853 - 0.675 \exp(-a_2/1.599), \\ X_{22} &= 0.949 - 0.233 \exp(-a_1/1.614). \end{aligned} \quad (7)$$

The calculated stresses are shown in Fig. 9. The stresses are negative, i.e., compressive, for both directions and saturate for larger coverages.

The experiment measures the stress difference $\Delta\tau_{1,2}$ between the mean stress $\bar{\tau}_{1,2}$ of a surface with (2×1) O domains and the stress $\tau_{\text{Cu},1,2}$ on the clean Cu(110) surface

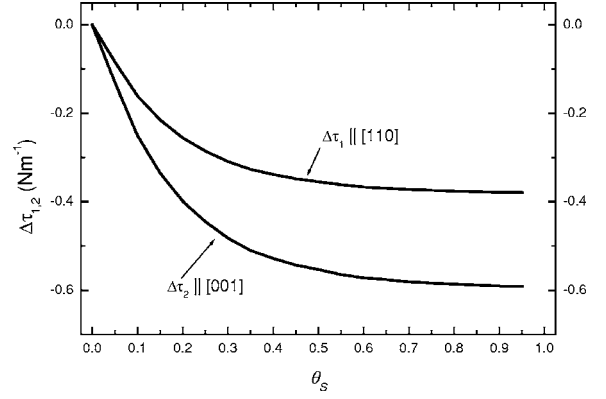


FIG. 9. Calculated stresses from the bending of Fig. 8 and Eq. (6) in the labeled directions plotted vs the coverage. The stresses are negative, i.e., the adsorption of oxygen induces a compressive stress.

$$\Delta\tau_{1,2} = \bar{\tau}_{1,2} - \tau_{\text{Cu},1,2}. \quad (8)$$

The averaged stress $\bar{\tau}_{1,2}$ is the coverage-weighted sum of the stress on the oxygen covered areas and the clean surface

$$\bar{\tau}_{1,2} = \tau_{\text{O},1,2}\theta_s + \tau_{\text{Cu},1,2}(1 - \theta_s). \quad (9)$$

For the stress induced self-assembly $\tau_{\text{O},1,2} - \tau_{\text{Cu},1,2}$ is the relevant quantity, which is

$$\tau_{\text{O},1,2} - \tau_{\text{Cu},1,2} = \Delta\tau_{1,2}/\theta_s. \quad (10)$$

For the $[1\bar{1}0]$ direction, i.e., orthogonal to the oxygen stripes $\Delta\tau_{[1\bar{1}0]}/\theta_s$ can be identified with the so-called line force monopole $f_{[1\bar{1}0]}$. The experimental data can be fitted in this $[1\bar{1}0]$ direction by $f_{[1\bar{1}0]} = \Delta\tau_{[1\bar{1}0]}/\theta_s \approx -0.24 - 1.7e^{-2.5\theta_s} \text{ N m}^{-1}$, and in the direction parallel to the stripes ([001] direction) by $\Delta\tau_{[001]}/\theta_s \approx -0.37 - 2.65e^{-2.5\theta_s} \text{ N m}^{-1}$ (Fig. 10).

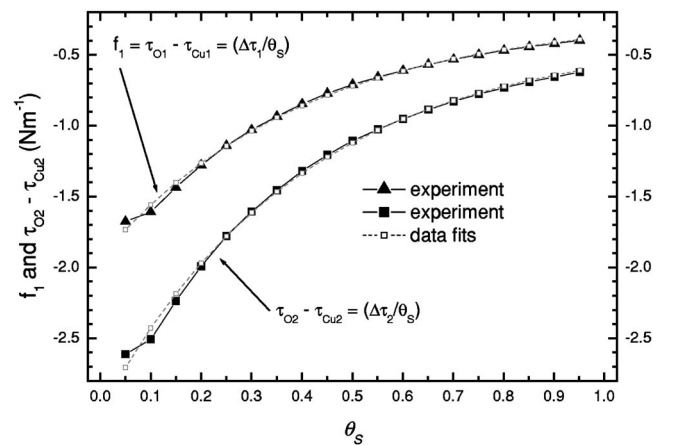


FIG. 10. Calculated stress differences divided by the coverage from Fig. 9. In the $[1\bar{1}0]$ direction, i.e., orthogonal to the stripes, this magnitude is equivalent to the so-called line force monopole $f_{[1\bar{1}0]}$.

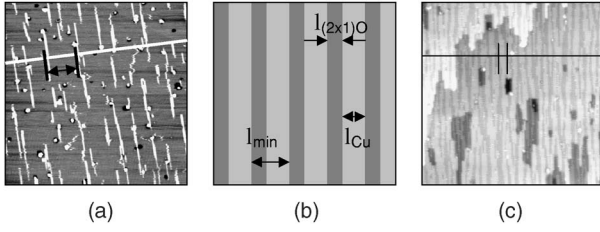


FIG. 11. The stripe periodicity is defined by $l_{\min} = (l_{(2 \times 1)O} + l_{Cu})_{\min}$ as illustrated in (b). The determination is performed by analyzing line profiles of STM images as illustrated exemplarily in (a) and (c).

VI. EXPERIMENTAL RESULTS AND DATA ANALYSIS, PART II: INVESTIGATIONS TO THE STRIPE PERIODICITY

As already mentioned one of the nice features of the technique used in these experiments is that it offers the possibility to determine stress, coverage, and spatial arrangement of stripes on the same sample. By analyzing the STM images in a wide range of coverages, we have determined the average distance l_{\min} as illustrated in Fig. 11 by analyzing line profiles as indicated in Figs. 11(a) and 11(c). For a perfect periodic stripe pattern l_{\min} would be the periodicity length. The index “min” is a reminder that in the classical theory of Alerhand *et al.*⁹ the stripe periodicity for the equilibrium structure results from the minimization of the domain wall energy and the elastic energy at constant coverage.

Our results for l_{\min} are plotted in Fig. 12 as open squares. Each data point in Fig. 12 was extracted from one STM image. The error bars represent the uncertainty of the arithmetic mean value. In general, the relative uncertainties of the mean values are significant smaller than 10%, which is quite satisfying. Qualitatively speaking this means that in a section of $100 \times 100 \text{ nm}^2$ of the surface the coverage and the stripe periodicity is rather nicely determined. The standard devia-

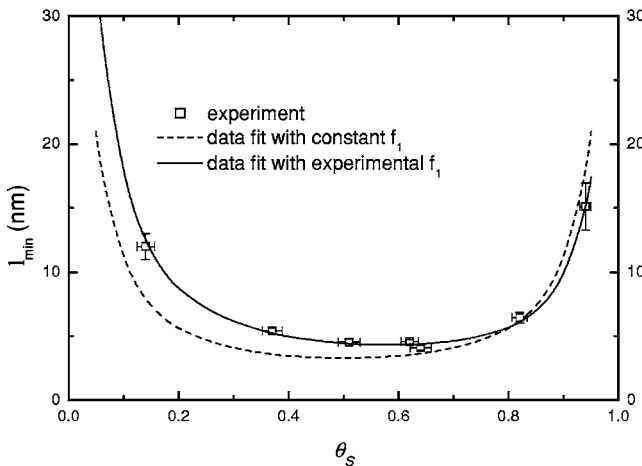


FIG. 12. Experimental data points of the stripe periodicity l_{\min} vs the coverage, respectively. Two fits according to Eq. (13) are performed with the experimentally observed force monopole (solid line) and with a coverage independent force monopole (dashed line).

tions, which denote the uncertainty of a single measurement, are comparable large (32–52 %). The relative uncertainty of a single measurement of the coverage is rather large (71%) for a very small coverage (0.14) but decreases with increasing coverage. We attribute these uncertainties to kinetic limitations of the ordering process at room-temperature exposure, which are especially pronounced at low coverages, probably due to the nucleation process. To obtain improved equilibrium structures one usually anneals the sample to, e.g., >450 K or exposes directly at higher temperatures.⁶

In the case of thermal equilibrium the theory of Alerhand *et al.*⁹ predicts a stripe periodicity

$$l_{\min} = (l_{(2 \times 1)O} + l_{Cu})_{\min} = \frac{2\pi a_c}{\sin(\pi\theta_s)} e^{(1+2\beta/C_2)}, \quad (11)$$

with a_c a constant of the order of an atomic distance, β the domain wall energy per length, and $C_2 = 2f_{[110]}^2 - (1 - \nu^2)/\pi Y$. Here again ν and Y denote the Poisson number and Young’s modulus, respectively. If one assumes the force monopole $f_{[110]}$ to be independent of the fractional coverage with stripes, as was done in previous analyses,⁷ l_{\min} is a symmetric function of the coverage. The dashed line represents an optimum fit assuming a constant force monopole. This fit is clearly at variance with our experimental data, which can be attributed to the kinetic limitations of the ordering. Nevertheless, assuming that the order of stripes is at least close to equilibrium and knowing that the minimum in the energy is extremely shallow² and therefore only little affected by some disorder, we apply equilibrium theory also to our data with less well-ordered stripes. With the force monopole obtained in our experiments

$$f_{[110]} = -0.235 - 1.7 \exp(-2.5\theta_s) \text{ N/m}, \quad (12)$$

l_{\min} becomes

$$l_{\min} = \frac{2\pi a_c}{\sin(\pi\theta_s)} \exp \left\{ 1 + \frac{\hat{\beta}}{f_{[110]}^2(\theta_s)} \right\}, \quad (13)$$

in which $\hat{\beta}$ is

$$\hat{\beta} = \frac{\pi\beta Y}{1 - \nu^2}. \quad (14)$$

With the coverage-dependent force monopole, Eq. (13) can be fitted to the experimental data in Fig. 12 with a_c and $\hat{\beta}$ as free variables. This fit procedure delivers $a_c = 3.2 \text{ \AA}$ and $\hat{\beta} = -0.108 \text{ N}^2 \text{ m}^{-2}$ (solid line). The negative value for $\hat{\beta}$ implies a negative domain wall energy β , which can be estimated to $\beta = -0.16 \text{ meV/\AA}$. This unexpected result does not depend on the details of the fitting procedure. A negative domain wall energy would mean that energy is gained when a single domain is split into two domains, which is equivalent to repulsive interaction between the CuO strings. It would imply therefore that the assembly of single CuO strings into domains would already be a result of the minimization of the total energy, including the elastic energy. In other words, in the absence of elastic forces the stable configuration for low oxygen coverage would be that of isolated Cu-O-Cu-O

TABLE III. Comparison of the experimental determined line force monopole vs the coverage from Ref. 10 and Fig. 10.

θ_S	0.51	0.56	0.58	0.76
$f_{[1\bar{1}0]}/\text{Nm}^{-1}$ (from Ref. 10)	-0.92	-1.05	-0.93	-1.01
$f_{[1\bar{1}0]}/\text{Nm}^{-1}$ (our results —Fig. 10)	-0.71	-0.65	-0.63	-0.49

chains. A calculation of assumed repulsive dipole-dipole interactions between the CuO strings delivers an energy in the right order of magnitude and could therefore provide a possible physical interpretation of a negative boundary energy.

VII. DISCUSSION

As already mentioned in the Introduction, the group of Prévot *et al.*^{10,11} performed a comprehensive study on the same system, albeit with a different method. Table III presents a comparison of the line force monopole $f_{[1\bar{1}0]}$ obtained by Prévot *et al.*¹⁰ to our own results. We find a qualitative agreement, i.e., the force monopole is negative, which corresponds to a compressive stress induced by the adsorption of oxygen on copper. In the small coverage interval investigated, Prévot *et al.* find a coverage independent force monopole of -1.0 N m^{-1} . Our values for the force monopole in the same coverage range are only a bit smaller with a mean value of approximately -0.6 N m^{-1} . The average over all data in Fig. 10 yields a mean of -0.9 N m^{-1} . Considering the completely different approaches, the quite sophisticated analysis of Prévot *et al.*, and the experimental errors the overall agreement is quite pleasing.

The stress data of Prévot *et al.* from Table III are based on measurements on samples, which have been exposed to oxygen at 600 K.¹⁰ In our experiments, the adsorption of oxygen took place at room temperature. As the evaluation of the stress data does not depend on the assumption of an equilibrium structure, we do not believe, that different preparation conditions are responsible for this deviation of the results.

In order to discuss the issue of stripe ordering, we first compare our data on $l_{\min}(\theta_S)$ to corresponding results of Prévot *et al.*, likewise obtained after room temperature exposure.¹¹ Figure 13 displays the data on $l_{\min}(\theta_S)$ obtained by Prévot *et al.* (open triangles) to our own data (solid squares). The data agree quite well in both the asymmetry and the absolute values. This is remarkable insofar as our data are obtained by direct observation using the STM while the data of Prévot *et al.* were extracted from a diffraction experiment (SPALED). Unfortunately, Prévot *et al.* did not publish a complete $l_{\min}(\theta_S)$ for the striped phase obtained under the same condition at which the stresses were evaluated. The data on $l_{\min}(\theta_S)$ published by Kern *et al.*⁶ were obtained after oxygen adsorption at room temperature followed by annealing to 600 K. This data set shows a considerable deviation in the higher coverage range whereby the curve becomes more symmetric around $\theta_S=0.5$ (open squares in Fig. 13). The difference between the results of ours and of Prévot *et al.* on the one hand and of Kern *et al.*

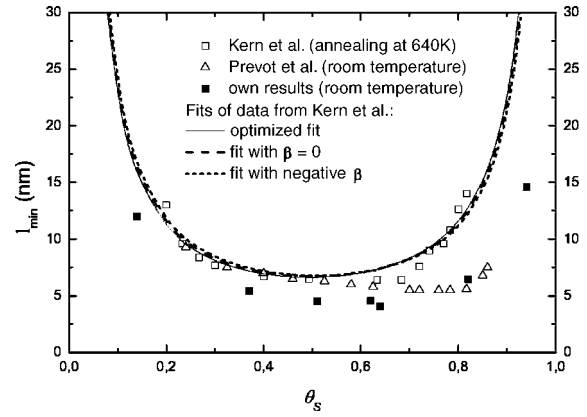


FIG. 13. Experimental data points of the stripe periodicity l_{\min} from different experiments vs the coverage, respectively. The data of Kern *et al.* are fitted with Eq. (13) by utilizing the coverage dependent force monopole $f_{[1\bar{1}0]}$ obtained in our experiments. The optimum fit, a fit with $\beta=0$ as well as a fit with a slightly negative β match quite well with the data points and among each other.

on the other suggests that the asymmetry of the $l_{\min}(\theta_S)$ curve is a consequence of kinetic limitations. In their recent work, Prévot *et al.* investigated the development of the apparent periodicity length at 308 K after oxygen exposure at 130 K.¹¹ They found that the periodicity length did develop slowly over a period of several hours, more slowly at high coverages, however, the resulting asymmetry appears to be the reverse of the asymmetry observed after oxygen exposure at 300 K; as far as one can tell from the published data. The question how the measured periodicity length $l_{\min}(\theta_S)$ is affected by kinetics in detail remains therefore open.

As a last point of the discussion we want to address the question of a possibly negative domain wall energy β . While the Marchenko-Alerhand model admits formally solutions with negative domain wall energies it is at least against intuition that they should be physical meaningful. In order to investigate whether a negative domain wall energy obtained by fitting our data to the Marchenko-Alerhand model is a consequence of the fact that our striped phases were not equilibrated we analyzed the equilibrated data of Kern *et al.*⁶ with Eq. (13) by utilizing the coverage dependent force monopole $f_{[1\bar{1}0]}$ obtained in our experiments. From the fit we obtain $a_c=3.8 \text{ \AA}$ and $\beta \approx +0.0161 \text{ meV/\AA}$. The optimum value for β , while being positive is close to zero, making the second term in the exponent of Eq. (11) practical zero. Because of this, the optimum fit describes the symmetric shape of the data quite well, despite the strong coverage dependence of force monopole. An equally good fit to the data of Kern is obtained for $\beta=0$ or for a slightly negative domain wall energy, e.g., $\beta=-0.0161 \text{ meV/\AA}$, which is also demonstrated in Fig. 13. This leaves us with a puzzle. Either the formal solution of the Marchenko-Alerhand model is valid also for small and possibly negative $2\beta/C_2$ or the equilibrated stripe phase which was believed to be the prototype for a Marchenko-Alerhand self-assembly is not described by the lowest order continuum approach of Marchenko and Alerhand.

VIII. SUMMARY

We have shown in detail how one can measure adsorbate induced surface stresses on electrically conducting samples using the bending bar technique and employing an STM for the detection of the bending as well as for studying the local structure of the surface. The advantage of this experimental approach is, that stress and surface morphology can be probed simultaneously. We have applied this method by measuring the oxygen induced surface stress on Cu(110). The magnitude $\Delta\tau_{[1\bar{1}0]}/\theta_s$, which equals the force monopole in the currently accepted theoretical model of self-assembly, agrees qualitatively with the results of Prévot *et al.*¹⁰ obtained by an entirely different approach. Contrary to Prévot

et al. we find that the force monopole depends significantly on the fractional coverage of the surface with oxygen stripes. Furthermore, data of the stripe periodicity are determined from STM images and plotted against the coverage. The asymmetric shape of the curve is most likely explained by kinetic limitations at room temperature. The possible existence of a negative domain wall energy is discussed.

ACKNOWLEDGMENTS

The very skillful preparation of the ultrathin Cu(110) single crystal bars by Udo Linke is gratefully acknowledged. One of the authors (M. Moiseeva) acknowledges the support by the DFG.

¹D. Sander, *Curr. Opin. Solid State Mater. Sci.* **7**, 51 (2003).

²H. Ibach, *Surf. Sci. Rep.* **29**, 193 (1997).

³H. Ibach, *Surf. Sci. Rep.* **35**, 71 (1999).

⁴D. Sander and H. Ibach, in *Landolt-Börnstein: Numerical Data and Functional Relationships in Science and Technology, New series, Group III: Condensed Matter*. (Springer, Berlin, 2002), Vol. 42, Pt. A2, p. 1.

⁵R. M. Tromp and J. B. Hannon, *Surf. Rev. Lett.* **9**, 1565 (2002).

⁶K. Kern *et al.*, *Phys. Rev. Lett.* **67**, 855 (1991).

⁷P. Zeppenfeld *et al.*, *Phys. Rev. Lett.* **72**, 2737 (1994).

⁸V. I. Marchenko, *Sov. Phys. JETP* **54**, 605 (1988).

⁹O. L. Alerhand *et al.*, *Phys. Rev. Lett.* **61**, 1973 (1988).

¹⁰G. Prévot *et al.*, *Surf. Sci.* **549**, 52 (2004).

¹¹G. Prévot and B. Croset, *Thin Solid Films* **428**, 25 (2003).

¹²G. Stoney, *Proc. R. Soc. London, Ser. A* **82**, 172 (1909).

¹³L. H. He and C. W. Lim, *Surf. Sci.* **478**, 203 (2001).

¹⁴W. A. Brantley, *J. Appl. Phys.* **44**, 534 (1973).

¹⁵H. Ibach and H. Lüth, *Festkörperphysik Einführung in die Grundlagen* (1999).

¹⁶K. Dahmen, S. Lehwald, and H. Ibach, *Surf. Sci.* **446**, 161 (1999).

¹⁷K. Dahmen, H. Ibach, and D. Sander, *J. Magn. Mater.* **231**, 74 (2001).

¹⁸K. Dahmen, *Induzierte Spannungen an Einkristalloberflächen* (Diss. RWTH Aachen, Jül-Bericht 3981, 2002).

¹⁹U. Linke (private communication).

²⁰G. Ertl, *Surf. Sci.* **6**, 208 (1967).

²¹D. J. Coulman *et al.*, *Phys. Rev. Lett.* **64**, 1761 (1990).

²²F. Jensen *et al.*, *Phys. Rev. B* **41**, 10233 (1990).

²³Y. Kuk *et al.*, *Phys. Rev. B* **41**, 12393 (1990).